Rheologica Acta Rheol Acta 33:1–21 (1994)

Original Contributions

A new elongational rheometer for polymer melts and other highly viscoelastic liquids[1,2])

J. Meissner and J. Hostettler

Eidgenössische Technische Hochschule (ETH) Zürich, Institut für Polymere, Zürich, Switzerland

Abstract: In polymer melt elongational rheometry only by the rotary clamp technique large elongations can be obtained homogeneously. However, as described in this paper, there still remain disadvantages that led to the development of a new rheometer with the following main features: The dimensions of the required sample are small ($60\times7\times2$ mm^3), the sample is supported by a cushion of inert gas and, after having reached the test temperature of up to well above 300 °C, it can be extended by a new type of clamps that make use of metal conveyor belts. The resulting tensile force is measured with a resolution of better than 100 mgf (0.001 N). The strain rate range is $0.001-1\,s^{-1}$, and the maximum Hencky strain is 7, corresponding to a maximum stretch ratio of 1100. Within the sample, the temperature variation in time and space is less than 0.1 °C. For the evaluation and documentation of the test performance, a video camera records the top and side views of the sample that carries a marking powder to permit the evaluation of the true strain rate. The operation of the instrument is easy, and so is the sample preparation, but care must be taken concerning the necessary isotropy and 'internal homogeneity'. Examples of test results are given for several polymer melts at various temperatures: (1) Polystyrene up to a total Hencky strain larger than 7 at 170 °C, (2) several types of polyethylene (LDPE, LLDPE, HDPE) at 150 °C, (3) poly(amide) at 250 °C, and (4) poly(ethersulfone) at 350 °C. The wide applicability of the new rheometer is demonstrated by adding results obtained from samples of bread dough. The surface tension has no influence on the results if an error of 3% can be tolerated. From the results it follows that by means of the newly developed rheometer many problems in polymer melt elongation have been solved.

Key words: Polymer melt elongation – elongational rheometry – instrumentation – polystyrene – polyethylene – poly(amide) – poly(ethersulfone) – bread dough

1. Introduction

Polymer melt elongation is one of the most important deformations in polymer processing. It is the dominant deformation in melt spinning, film and bottle blowing, and in the biaxial stretching of extruded sheets. In other polymer processing operations the last step before solidification is often an elongational deformation resulting in molecular orientation and anisotropy of the end-use properties of the final products. A second relevance of melt elongation is to production control and polymer science; melt elongational data are useful for polymer characterisation, because they are very sensitive to the molecular structure of a polymeric system. This is true not only for thermoplastic homopolymers but also for more complex polymeric systems. A third use of elongational data is in the evaluation of theories of polymer melt flow. The question of whether any constitutive equation is of general validity can only be answered by comparing its predictions with experimental data that include not only the viscosity and the viscometric functions, measured in shear, but also other types of deformation, including various modes of elongation.

[1]) Dedicated to Professor Dr. Hermann Janeschitz-Kriegl on the occasion of his 70th birthday.

[2]) Extended version of a paper presented at the XIth International Congress on Rheology, Brussels, Belgium, August 17–21, 1992.

However, in spite of this practical and theoretical relevance, there are very few laboratories world-wide in which polymer melt elongation is being studied. The situation can best be described by the fact that until now no scientifically sound elongational rheometer for polymer melts has been commercially available. The conventional tensile testing machines used to study the elongational behaviour of metals or solid polymers are inadequate for polymer melts for the following reasons:

1) Polymer melts are liquids, so they yield to the clamping forces within the clamps.
2) Due to gravity the sample changes its shape and flows away in a conventional tensile testing machine.
3) Polymer melt samples can be elongated a thousand times their initial length and even more. A conventional tensile testing machine limits the total strain applicable and, therefore, does not allow one to investigate the material behaviour at extremely large strains.
4) Conventional testing machines mostly operate with a constant increase of the sample length with time. It is not general practice that electronic controls are available to perform the exponential increase of the sample length, as is required for elongation with a constant time derivative of the Hencky strain in order to determine the elongational viscosity $\mu(t)$.

The investigation of polymer melt elongation started around 1970. Of the very early papers we cite only Jenckel and Überreiter (1938), Karam and Bellinger (1964), Ballman (1965), Cogswell (1968), and Vinogradov et al. (1969). It is remarkable that many such studies, including the development of the measuring techniques, were performed in industry. For a review of the experimental as well as the theoretical aspects we refer to the monography by Petrie (1979). Previous to the development of the technique described in this paper, only by the rotary clamp technique could large elongations be achieved that were homogeneous so that the forces acting on the clamps could be used for a reliable stress measurement. The development of the rotary clamp technique for simple elongation, as well as for different modes of multiaxial elongation, has been described in several publications by Meissner (1969, 1972a, 1985, 1987, 1992a) and by Meissner et al. (1981, 1982).

However, there are drawbacks with the rotary clamp technique, viz. the large size of the samples, the need of a supporting liquid that sometimes has a physical-chemical interaction with the polymer melt, and the upper temperature limit of (at most) 200 °C that excludes important polymer melts from being investigated. All these difficulties (and more) are resolved in the new rheometer that makes use of metal conveyor belts instead of rotary clamps. The sample size is reduced, and the sample preparation is simplified. Instead of using a supporting liquid the sample is supported by a cushion of inert gas, and the maximum temperature used so far has been 350 °C. The total test performance can be easily recorded, controlled and documented by use of a video system.

In this paper, after the necessary definitions we start with a brief description of the rotary clamp technique from which the concept of the new rheometer was developed. This is followed by a description of important design details, the rheometer specifications, and our experience concerning the preparation of samples. Finally, examples of test results are given that demonstrate the excellent resolution of the new rheometer, the high temperature range, and its broad applicability. Results are reported for melts not only of polystyrene and polyethylene, but also of polyamide and polyethersulfone. As an example of a completely different class of materials, test results obtained in the new rheometer for samples of bread dough are included.

2. Basic definitions

Because of the large strains involved in polymer melt elongation, it is important to state clearly which strain measure, ε, is being used. Its time derivative, $\dot{\varepsilon}$, is kept constant during a simple elongational test starting at $t = 0$ such that

$$\dot{\varepsilon}(t) = \dot{\varepsilon}_0 h(t) \ , \tag{1}$$

where the unit step function is

$$h(t) = \begin{cases} 0 (t<0) \\ 1 (t>0) \end{cases} . \tag{2}$$

The current tensile stress $\sigma(t)$, divided by the constant strain rate $\dot{\varepsilon}_0$, defines the elongational viscosity

$$\mu(t) \equiv \sigma(t)/\dot{\varepsilon}_0 \ . \tag{3}$$

Obviously, different strain measures lead to different time derivatives, defining different test procedures and resulting in different definitions of what is called *elongational viscosity*[3]). The most widely used strain

[3]) This conclusion touches a fascinating, much more fundamental question. The interested reader is referred to Zülle et al. (1987) and to Dealy (1990).

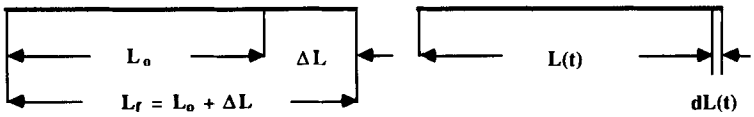

$$\lambda = L_f / L_0$$

$$\varepsilon^C = \Delta L / L_0 = \lambda - 1$$

$$d\varepsilon^H = dL(t) / L(t)$$

$$\varepsilon^H = \int d\varepsilon^H = \int_{L_0}^{L_f} dL/L = \ln (L_f / L_0) = \ln \lambda.$$

Fig. 1. Definition of strain measures ε^H (Hencky) and ε^C (Cauchy) by stretching a rod of initial length L_0 to final length L_f. λ is called the *stretch* or *stretch ratio*

measures are the Cauchy (or engineering) strain ε^C and the Hencky strain ε^H. These are related to the *stretch* or *stretch ratio* λ as indicated in Fig. 1. If a strand of initial length L_0 is stretched to a final length L_f the definition of the stretch is

$$\lambda \equiv L_f / L_0 \ . \tag{4}$$

In this paper we use the Hencky strain as our strain measure so that

$$\varepsilon \equiv \varepsilon^H \ , \tag{5}$$

and the time derivative is $\dot{\varepsilon} \equiv \partial \varepsilon^H / \partial t$.

In fluid dynamics the strain rate tensor is defined as

$$\boldsymbol{D} \equiv \frac{1}{2}(\nabla \boldsymbol{v} + \nabla \boldsymbol{v}^{\mathrm{T}}) \ , \tag{6}$$

where $\boldsymbol{v}$ is the velocity, $\nabla \boldsymbol{v}$ the velocity gradient, and $\nabla \boldsymbol{v}^T$ its transpose. For simple elongation in the direction x_1, it can be shown that the first principal component of the strain rate tensor is the time derivative of the Hencky strain in the direction x_1: $D_{11} \equiv \dot{\varepsilon}_{11} = \dot{\varepsilon}_0 h(t)$, and that for incompressible liquids which we consider here the strain rate tensor is

$$\boldsymbol{D}(t) = \dot{\varepsilon}_0 h(t) \begin{pmatrix} 1 & 0 & 0 \\ 0 & -0.5 & 0 \\ 0 & 0 & -0.5 \end{pmatrix} \ . \tag{7}$$

For such a test, when the original specimen has the shape of a bar or rectangular cross-section, it increases in length and decreases in the cross-sectional area exponentially with time. This change of bar dimensions is illustrated in Fig. 2.

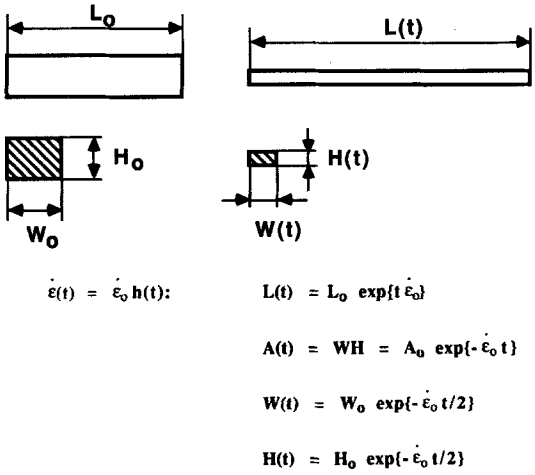

Fig. 2. Elongation of a sample of rectangular cross-section. Change of dimensions due to a step function strain rate $\dot{\varepsilon}_0$ in the direction of the sample length for incompressible material

3. Rheometer concept

The roots of the new rheometer go back to the first version of the rotary clamp design first published in 1969 and illustrated in Fig. 3. In the rotary clamp

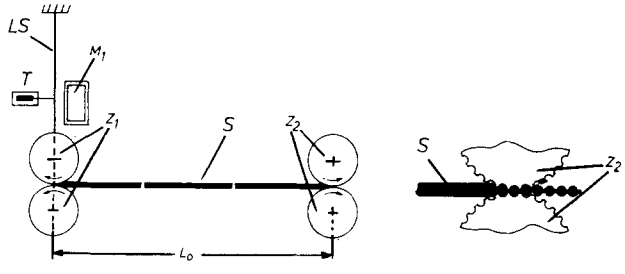

Fig. 3. Schematic diagram of the first version of the rotary clamp elongational rheometer for polymer melts (Meissner, 1969)

rheometer the polymer melt sample S is a strand of circular of rectangular cross-section. This strand floats horizontally on a bath of silicone oil that compensates for the weight of the melt by buoyancy and keeps the sample at the desired test temperature. The sample S is clamped at each end by a pair of toothed rollers ('rotary clamp'). These clamps, Z_1, Z_2, have a fixed distance L_0 between them and rotate in opposite directions. As a result, the melt is transported out of the zone L_0 such that the material between the rotary clamps is elongated homogeneously and, if the speed or rotation of the rollers is kept constant, with constant 'Hencky strain rate' (abbreviation for *constant time derivative of the Hencky strain*) as is required for the determination of $\mu(t)$. As the deformed melt within the clamps is immediately transported out of the zone L_0 (distance between the clamps), the deformation of the melt strand remaining within L_0 is homogeneous. There is no necking of the sample at the clamps, in contrast to the necking of samples when conventional clamps are used. The dimensions of the apparatus do not limit the maximum strain. In fact, total Hencky strains of $\varepsilon_{max} = 7$ can be obtained corresponding to a stretch ratio of $\lambda_{max} = 1100$ (Meissner et al., 1981), and even larger total strains have been obtained more recently.

As is shown in the schematic diagram of Fig. 3, the left-hand rotary clamp Z_1 together with its driving motor M_1 is positioned at the free end of a leaf spring LS. The essential idea is that the torque for squeezing the melt within the clamp is compensated by a counter-torque from the motor, such that the position of the free end of the leaf spring is not changed by any torque required, because the motor and clamp form a closed mechanical system. The only force acting to deflect the leaf spring is the force $F(t)$ that is exerted by the sample on the clamps during deformation. The result is a corresponding deflection of the leaf spring. This deflection is measured by a LVDT (denoted by T in Fig. 3) and, after calibration, provides the signal for the determination of the force $F(t)$.

The application of the rotary clamp technique has brought important new insight into the elongational behaviour of polymer melts, especially for low density polyethylene with its remarkable contrast in the behaviour of the elongational viscosity as compared with the shear viscosity, as reported first by Meissner (1971, 1972b) and later by Münstedt and Laun (1979).

In spite of the progress obtained by the rotary clamp technique in polymer melt elongational rheometry, there still remained the following difficulties:

1. The circumferential speed of the clamps is not completely transferred to the local speed of the sample at the location of clamping. The resulting 'strain rate lag' has to be determined experimentally in a separate experiment. The determination of the true elongation is elaborate but necessary in order to avoid large errors in the stress $\sigma(t)$, especially at large strains (Meissner et al., 1981).
2. In order to minimize the error, large samples of 60 – 80 cm length are required that must be isotropic and of homogeneous cross-section. The preparation of large samples is not easy; when extruded rods are applied, they shrink on melting. The extrusion of straight rods is sometimes impossible, because during the (inhomogeneous) cooling the rods bend due to the large coefficient of thermal expansion. According to our recent experience with blends of polystyrene/polymethylmethacrylate (Meissner, 1992b) the best, i.e. the most isotropic and homogeneous samples are prepared by extruding the required amount of polymer as a melt in a twin-screw extruder and, without cooling, inserting this melt into a press for compression moulding flat sheets out of which the samples are milled.
3. The floating of the sample on a supporting liquid excludes many polymers from such tests because of physical-chemical interactions between the melt and the supporting liquid.
4. The maximum temperature is limited because of the supporting liquid, thus excluding important polymer melts from study. Consequently, there are few data in the literature concerning elongational behaviour measured at temperatures above 200 °C.
5. The test performance must be verified, especially at large elongations, as has been pointed out by Meissner et al. (1981), and this is laborious with the rotary clamp technique.

These difficulties inspired a complete revision of the elongational technique and resulted in the concept of the new rheometer shown schematically in Fig. 4. The individual characteristics of the new rheometer are as follows:

1. The rheometer housing RH is a relatively small box (inner dimensions: 280 mm long, 80 mm deep, 220 mm high) formed by six metal plates into which electrical heater wires are imbedded. The inner sides of the plates are blackened to help generate a homogeneous temperature field inside the rheometer housing by means of radiation, especially at higher temperatures.

2. A new type of clamp is the central feature of the new design. The two toothed rollers of the rotary clamp used in the previous apparatus are replaced by two metal conveyor belts MB. The belts move on belt fixtures BF that sit on fixture carriers FC from which they can be removed for cleaning. The upper fixture carrier can be lifted by a knob KC on top of the housing via a chain CUB. On lifting CUB the upper belt is lifted, and the clamp is thus opened from outside the housing. The metal belts satisfactorily transfer the velocity of the belts to the local speed of the sample S at the position of clamping such that there is practically no lag of the strain rate due to an incomplete velocity transfer.
3. One clamp (the right clamp in Fig. 4) is mounted on the lower ends of two parallel leaf springs LS. The upper ends of the two leaf springs are together mounted to the same fixture fastened to the upper plate of the rheometer housing. This fixture guarantees a parallel displacement of the core inside the LVDT for the force measurement when the springs are bent by the tensile force exerted by the sample S on the clamps. To drive the metal belts, new light-weight motors M are mounted directly on the lower ends of the leaf springs by means of the motor housing connection MHC. Thus, the operating principle is the same as that used in connection with the left-hand rotary clamp of Fig. 3. As a result, very small forces can be measured with a high resolution, provided the oscillations of the force signal due to the natural frequency of the spring system are sufficiently damped either by the viscosity of the sample or externally by the oil damping device OD. The motor block M includes not only the motor but also a reduction gear set, an encoder, and a tachogenerator.
4. The oil bath previously used to support the sample is replaced by a cushion of nitrogen or argon gas on which the sample floats. The sample supporting system SSS consists of a table on top of which a flat metal frit is located. Compressed inert gas flows from the gas inlet GI into the table and from there through the frit to support the polymer melt sample. The temperature of this sample supporting gas cushion equals the test temperature. By this supporting technique, any influence of the environment on the sample is avoided, and the test temperature can be increased well above the previous limit of 200 °C.
5. The sample size is reduced, and the sample preparation is simplified. The sample shape used so far has been a bar of rectangular cross-section with the following initial dimensions: 60 mm long, 2 mm high, 7 – 8 mm wide. This corresponds to a total sample mass of approximately one gram. The deformation length L_0 (distance between the tips of the clamps) is 50 mm. Such samples can be easily cut or milled from carefully compression-moulded sheets.
6. The walls of the rheometer housing are electrically heated to the test temperature. Due to the high temperature sensitivity of the melt viscosities of some polymers, the temperature has to be controlled very precisely. Unfortunately, the driving motors and the LVDT must operate at much lower temperatures than the maximum test temperature. Therefore, they must be located outside the rheometer housing. This requires special care because of

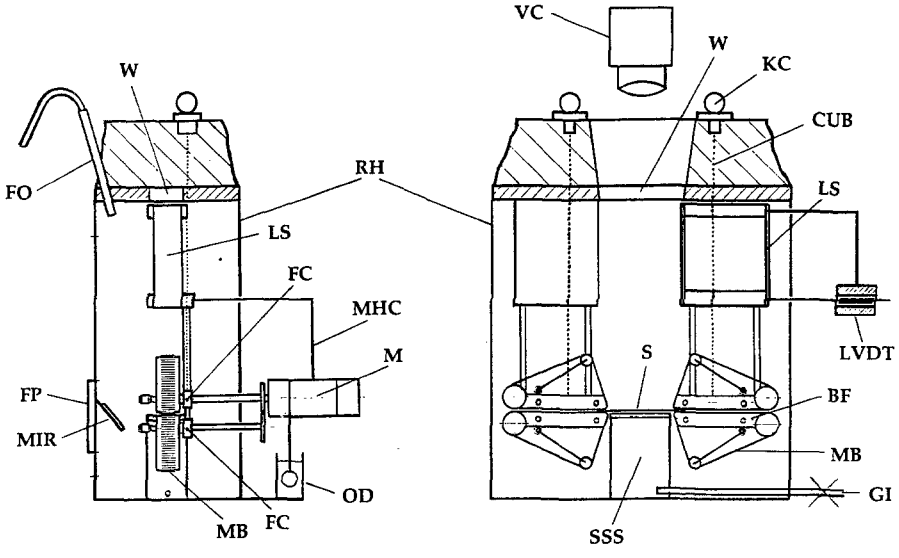

Fig. 4. Schematic diagram of the new elongational rheometer with clamping the sample by metal conveyor belts, supporting the sample by a gas cushion, and video recording the test performance

the thermal expansion of the connecting metal parts, and it requires openings in the rheometer housing. Through these openings the gas introduced for sample support can leave the housing.

7. The insertion of the sample into the rheometer is simple. When the test temperature is reached inside the rheometer housing (with the correct flow through GI of preheated inert gas) the knobs KC (Fig. 4) are lifted, opening the clamps. The front plug FP is replaced by a special feeding plug equipped with a feeding tool for inserting and precisely positioning the sample between the opened clamps. Then the plugs are exchanged, the knobs are released, and as soon as the sample has reached the test temperature, the test can be started.
8. It is vital that the quality of the test performance be verified. For this purpose markers can be used or a grid can be printed on top of the sample S. The sample is illuminated through outlet FO by a fibre optic system, and can be photographed through window W during elongation not only from the top but also from the side. The side view is reflected through the window W by means of the mirror MIR. By analyzing the location of the same marks at different instances during the deformation period, monitoring of test performance is possible.
9. For monitoring and documenting the test, we make use of a video system. It consists of a light source and a glass fibre cable, the mirror MIR (Fig. 4) for the side view of the sample inside the rheometer housing, the video camera VC, a video recorder, a timer that reports the current test time to the video recorder, a video screen, and a thermoprinter to provide individually selected pictures from the video tape.

Figure 5 is a view of the central part of the rheometer with the two clamps, each of which makes use of two metal conveyor belts. The two clamps hold a sample of solid polystyrene, on top of which a grid is printed. This picture was taken at room temperature, with the front door of the rheometer open. Below the sample, the supporting table with the frit for the gas outlet is located. Above the sample we see a wire for fixing a platinum resistance thermometer that measures the test temperature near the sample.

Figure 6 shows the whole rheometer system. On the left can be seen the rheometer housing with its door closed. Above the rheometer, the video camera is installed and we also see the illumination system with the fiber optics connection. At the right side of the rheometer, there is the control unit for the gas stream used to support the sample, and the amplifier for the LVDT of the force measuring system. The video monitor shows the views from the top and from the side of the polystyrene sample of Fig. 5. The printed bar grid can be clearly seen. The side view of the sample is the white strip above the numbers. These numbers are used for test identification, and they record the current instant of the deformation time.

4. Design details and rheometer specifications

The most important feature of the new rheometer is the sample clamping mechanism which consists of metal conveyor belts. Figure 7(a) shows one of the belt fixtures, which can be inserted into a fixture carrier (FC of Fig. 4) by means of two holes. A special tool allows one to insert the belt fixture into the instrument and to take it out after the test, even at high temperatures. Each fixture consists of a short slide plane of 10 mm length for the belt, the driving gear for the connection to the driving motor, and a spring-loaded guide wheel. Figure 7(b) shows the belt fixture carrying a conventional metal conveyor belt.

For melts of relatively low viscosity we found out that after melting, but before starting the test, the

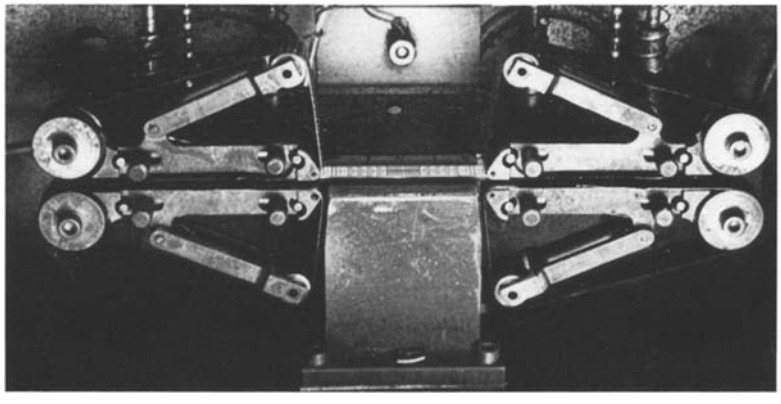

Fig. 5. Metal belt clamps within the rheometer housing clamping a (solid) polystyrene sample. A grid of bars is printed on top of the sample. Below the sample is the table of the sample supporting system, above the sample there is a wire fixture with a platinum thermoresistor

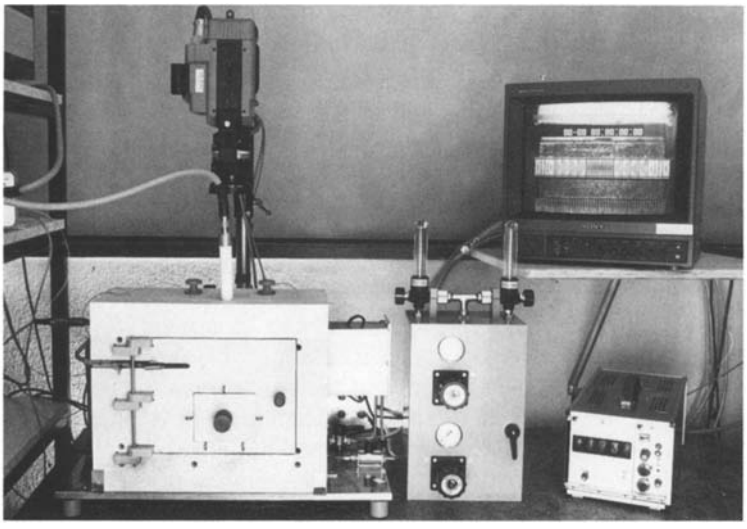

Fig. 6. View on the rheometer system with the rheometer housing, video camera and video screen, gas flow control for sample support and amplifier for the force measurement. On the screen, the sample of Fig. 5 is shown with the printed-on grid, below: seen from the top, above the numbers: seen from the side by means of the mirror MIR of Fig. 4

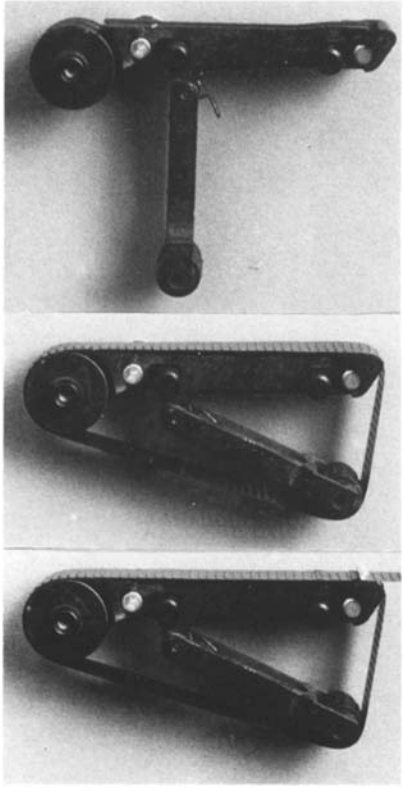

a) without belt

b) standard belt

c) special belt with tongue and distance pin

Fig. 7. Metal belt fixture (a) without belt, (b) with conventional belt, (c) with special belt to which a metal tongue is welded for bridging the gap between the clamp and the table of the sample supporting system. In (c) also the pin is shown that prevents too much squeezing of low viscosity samples before the test is started

melt may flow between the supporting table (SSS of Fig. 4) and the tips of the metal belts. Therefore, the latter were equipped with a tongue that is positioned such that at the insertion of the sample, the tongue bridges the gap between the table and the clamp. As soon as the test is started the tongues move with the sample ends into the clamps. Of course, for the very first portion of the deformation the motor speed has to be adjusted appropriately to take care of the initial change of the length L_0. A second observation was that with melts of low viscosity, the upper belt is pressed too quickly against the lower belt. In this case a pin of 1.5 mm diameter is positioned on the lower belt as shown in Fig. 7(c). When the test is started, this pin keeps the gap from being reduced too much until the pin is transported out of the small gap between the slide planes of the two belts and comes into a much wider opening between the belts.

Three different clamping situations are shown as silhouettes in Fig. 8: (a) the conventional clamping; (b) the clamping with the belts modified by the addition of tongues for low viscosity melts, and the pins between the slide planes, which is the situation at the start of the experiment; (c) the application of only the lower belts equipped with the tongues. The latter configuration is used when the polymer melt under test has a sufficiently low viscosity and sticks perfectly to the metal belts; but the advantage is that the oscillating mass of the spring system is reduced, increasing its natural frequency.

The dimensions of the belt length and the base distance L_0 are such that for one complete cycle of the belts the total strain of the material between the clamps is $\varepsilon_{max} = 7 (\lambda = 1100)$ when conventional belts

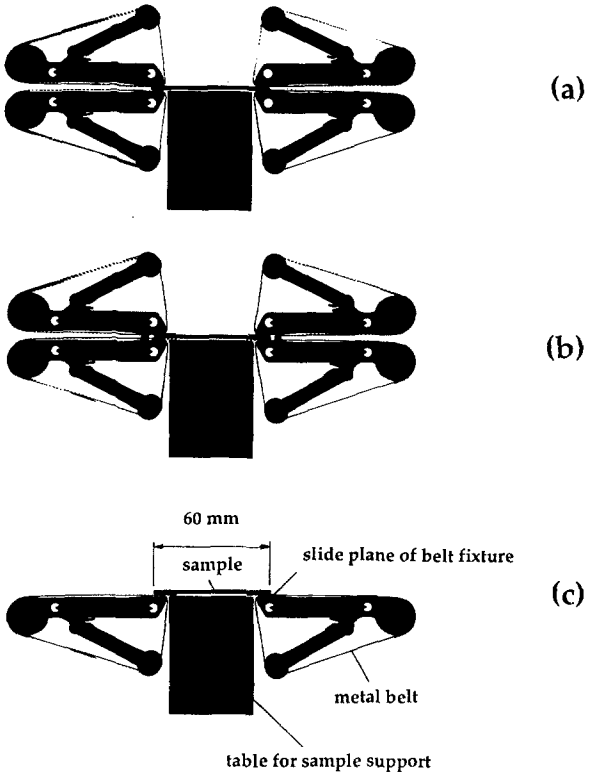

Fig. 8. Silhouettes of three types of clamping the sample between metal conveyor belts

are used. For the special belts with the welded-on tongues, the maximum strain is $\varepsilon_{max} = 6(\lambda = 403)$. This reduction of the maximum strain is caused by the fact that the tongues touch the sample-supporting table before a complete cycle of the belts is performed. However, this smaller ε_{max} does not seem to be a serious limitation, because for low viscosity melts (for which these belts are a must) even at the highest strain rate of $1\,s^{-1}$ the tensile force is small and quickly vanishes below the force resolution of 50 mgf.

The system for calibrating the force sensor is based on a weight-loaded balance and is shown in Fig. 9. Permanently mounted to the upper ends of the two leaf springs – as indicated by LS(UE) – is the balance carrier BC with the balance knife BK, which is located outside the rheometer housing RH. The lower ends of the leaf springs are connected to the core of the LVDT. This connection is marked by LS(LE) in Fig. 9 and is also shown in Fig. 4.

To calibrate the force measuring system, the balance beam BB is located with its lower notch on top of the balance knife BK. The moment of the balance beam itself is neutralized by the beam counter-weight BCW which is adjusted so that the tip of the LVDT-core nearly touches the lower arm of the balance beam. By hanging a deadweight F_w from one of the notches in the balance beam at a distance x_i from the balance knife, a moment $F_w x_i$ is exerted that is in equilibrium with a counter-moment Fh, where F is the force acting through the tip of the LVDT-core on the leaf spring system (LS of Fig. 4), and h is the perpendicular distance between the axis of the LVDT-core and the tip of the balance knife. Hence, the effective calibration force is $F = F_w x_i / h$. By varying x_i and F_w, a wide range of forces F can be applied to the leaf spring system for calibration.

The specifications of the new elongational rheometer are given in Table 1. Listed there are the strain rate range, the maximum strain, the range and resolution of the tensile force, and the temperature range. The compliance of the tensile force spring system is 260 μm/N. The sample dimensions are small. At room temperature the initital dimensions of a typical sample are: 60 mm long, 7 – 8 mm wide, and 2 mm thick.

Table 1. Specifications of the metal belt elongational rheometer

1. Strain rate range	$0.001 - 1\,s^{-1}$
2. Maximum strain (Hencky)	7 ($\lambda_{max} = 1100$)
3. Tensile force	$0.001 - 2\,N = 0.1 - 200\,cN$ ($\approx 0.1 - 200$ gf)
4. Temperature maximum Temperature constancy at sample	350 °C ±0.2 °C
5. Environment	Inert gas atmosphere
Recommendation	Analytical nitrogen or argon

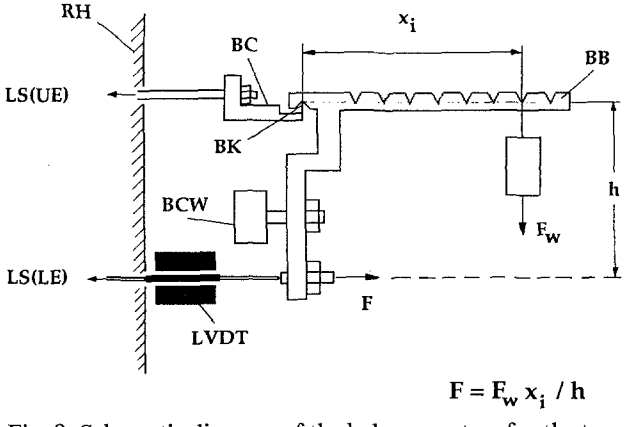

Fig. 9. Schematic diagram of the balance system for the tensile force calibration

5. Sample preparation and test procedure

In this section experimental details in performing the measurements are described that are vital to obtain reliable test results.

(a) Sample preparation

The quality of the test results depends not only on the quality of the instrument but also on the quality of the sample. At the beginning of a test the sample must be isotropic and externally as well as internally homogeneous. *External homogeneity* refers to a constant cross-sectional area independent of the length co-ordinate, whereas *internal homogeneity* means that the molecular connectivity is independent of location within the sample. The latter property cannot be taken for granted, especially when samples of high molecular weight are prepared from granules by compression moulding. If there is not adequate time for the molecules at the boundary between two granules to interdiffuse 'sufficiently' after melting, the connectivity of the molten polymer network within the sample is inhomogeneous. During elongation, this may result in an early fracture of the sample, giving a false indication of the elongational properties of the homogeneous melt.

We have found compression moulding to be the best method to achieve reasonable isotropy in the required flat sheets. In order to overcome the difficulties associated with the boundaries between granules we first shear in a twin-screw extruder or, if only a small amount of material is available, in a capillary rheometer[4]). After a sufficient amount of melt has been extruded, the extrudate is immediately transferred into the mould of the press. Thus, the compression moulding starts with a homogeneous hot melt and results in a homogeneous and isotropic sheet from which samples with the correct shape are milled. It had been our previous experience that only by such a procedure can very large total strains be achieved even with melts of linear polyethylene. The same procedure, when used for samples of polystyrene in the new rheometer, resulted in total strains of more than seven. For acceptable results in polystyrene melt rheology, it is essential that the granules before, and the finished samples after, compression moulding be kept under a vacuum, because air is dissolved in solid polystyrene and starts to form bubbles as soon as melting occurs.

[4]) High pressure capillary rheometer Rheograph 2000 of Göttfert GmbH; for the extrusion purpose we replace the piston by a screw equipped with a separate drive.

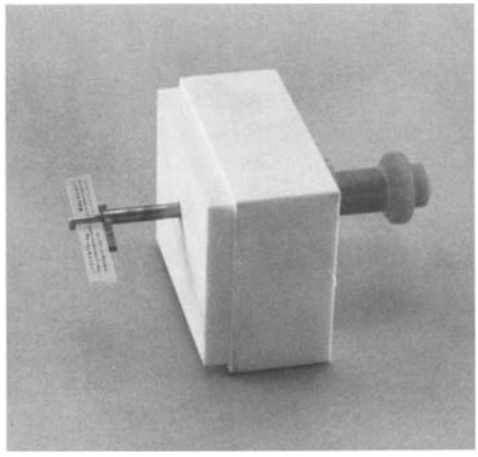

Fig. 10. Feeding plug for inserting the sample into the preheated rheometer

(b) Sample loading

When the test temperature is reached in the empty rheometer the clamps are opened by lifting the knobs KC of Fig. 4. The front plug (FP in Fig. 4) in the center of the door is replaced by the feeding plug shown in Fig. 10. This feeding plug allows one to insert the cold sample between the two clamps in the correct position. In its center, there is a spring-loaded fixture that can be moved along its axis. This fixture holds the sample during insertion into the instrument. The sample can be manipulated within the fixture by moving the knob shown at the right-hand side of the plug in Fig. 10. Through the top window of the rheometer housing the positioning of the sample can be observed on the video screen. As soon as the correct position is achieved, the sample is released by pressing the knob of the feeding plug so that it rests freely on the lower metal belts of the two clamps. Then the feeding plug is replaced by the original plug. After a heating-up period of 5 – 10 minutes the sample has reached the test temperature. When the knobs KC of Fig. 4 are released the measurement can be started.

(c) True elongational strain rate

For a precise evaluation of the measured tensile force, it is necessary to determine the 'true' strain rate, which may be different from the 'nominal' strain rate. The latter is calculated using the 'free length' L_0 of the sample[5]) between the clamps and

[5]) From visual inspection of the melt flow of the sample into the clamps, L_0 is defined to be 4 mm longer than the free distance between the tips of the clamps.

the velocity u of the metal bands: $\dot{\varepsilon}_{\text{nominal}} = 2u/L_0$. For the determination of the true strain rate, the sample is marked and the change in the distance between marks during elongation is measured. For this purpose the video camera of Fig. 4 records the test performance together with the current time of elongation, and from the video record, print-outs from the photoprinter are made.

Several methods were tried to apply marks, e.g. printing a grid on the sample or using a powder. As an example, Fig. 11 shows a sequence of several images from the video record made during the elongation of a polystyrene sample. Before inserting the sample into the rheometer, a grid of white colour had been printed on the sample. The first frame (top frame of Fig. 11) shows the sample resting on the two lower metal belts of the clamping system shortly before the deformation started. The upper metal belts are not yet in their operation positions because the knobs KC of Fig. 4 have not yet been released. The view from the top (below the frame identification number) shows the grid printed on the sample, the side view of the sample is above this number. The indicated time refers to the current time of elongation. We notice that for $t>0$, at the rim of each side view the clamping of the sample by the metal belts is visible. Thus, the video record shows the total length of the sample between the clamps. Because of the transparency of the polymer melt, the view from the top mainly shows the structure of the frit through which the supporting gas is flowing. The frames of Fig. 11, and more so the video movie made from each test, document the excellent homogeneity of the elongation[6]).

A printed-on grid, however, has two disadvantages, (i) at large deformations, there are few, if any, marks left on the sample, (ii) the dried colour, after printing, has a reinforcing effect. Therefore, especially when the viscosity of the sample is relatively low, an erroneous, higher viscosity is measured. Because of these disadvantages, another method of marking the sample was developed that turned out to be successful: We now apply silicium carbide (SiC)-powder of 20 μm particle size. The powder is applied to the top surface of the sample only along the center line by means of the tools shown in Fig. 12. The legend of Fig. 12 explains the marking procedure.

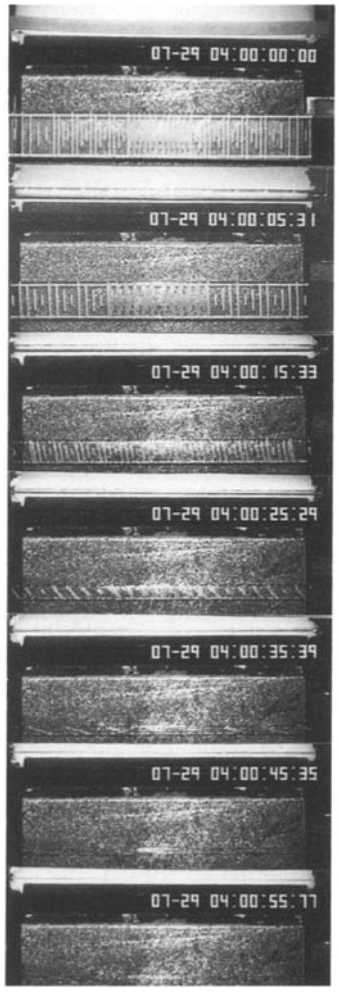

Fig. 11. Top and side views of a polystyrene sample during elongation with a strain rate of 0.1 s^{-1} at 170 °C. Material: Polystyrol 158 K of BASF, Ludwigshafen am Rhein, Germany. The sample was prepared by pre-extrusion followed by compression moulding. A grid of white colour was printed on the sample. The indicated times refer to the current instants of deformation at which the frames were recorded. The side view of the sample is above, the top view below the identification number. The morphology of the frit of the sample supporting device makes it difficult at very large strains to identify the sample from the top

A specially designed mask for the metal net produces the broad particle layer as shown in Fig. 12 only in the central part of the sample where more particles are needed, whereas away from the center near the clamping areas this layer is narrower. As an example of the evaluation of the true strain rate, Fig. 13 shows the side views of a sample of low density polyethylene during elongation at a nominal strain rate of 0.1 s^{-1} and a temperature of 150 °C. The SiC-particles can be

[6]) Because of printing problems the printed-on bars are not precisely perpendicular to the sample axis. This is the reason why with the elongational strain the bars increasingly change their slope. But what is important here is the visualization of the perfect homogeneous deformation.

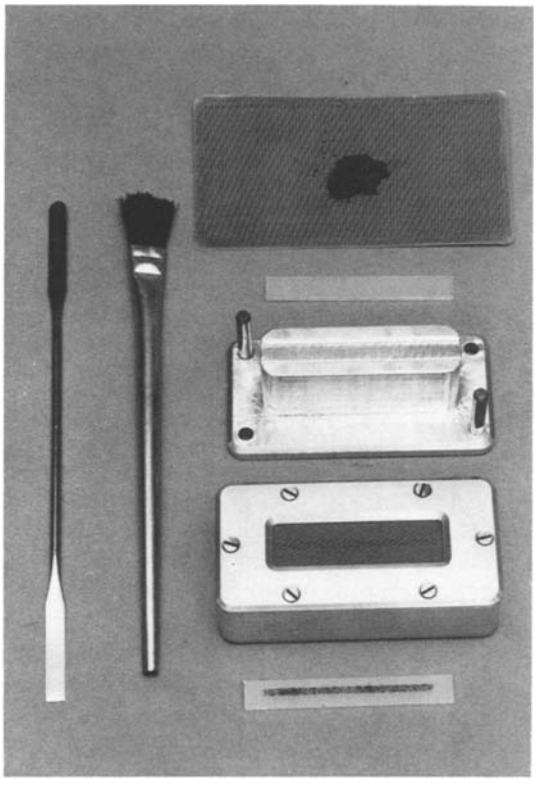

Fig. 12. Tools for applying SiC-powder to mark the polymer sample. Starting from the top is shown: Metal net (mash size 200 μm) with SiC-powder (particle size 20 μm), the compression moulded sample, the sample holder (here without sample), the cover for the sample after insertion into the slit of the sample holder. The cover has a small net and such a shape that on applying the marking powder only a small strip along the center-line of the sample is marked. The result is the sample with markers as shown at the bottom of the figure

Fig. 13. Determination of the true strain rate by the 'particle tracking method'. The distances of the same two particles i – i are measured at two different instants of the deformation and reveal the strain rates given in the last column of Table 2. Material: Low density polyethylene (Lupolen 1810 H of BASF, Charge 681133259). Test conditions: Temperature 150 °C, nominal strain rate 0.1 s^{-1}

clearly seen and the same particles can be followed during replaying of the video record. The last four digits of the identification number of each frame refer to the current time of elongation, t, e.g. the first frame corresponds to $t = 2.59$ s. For the last frame, at $t = 48.61$ s, the view from the top on the sample is also shown (below the identification number).

The distances between the two particles 1 – 1 in the first and second frames of Fig. 13 are 55.7 and 87.5 mm, respectively[7]). This implies a stretch $\Delta\lambda = 1.576$ and correspondingly a strain $\Delta\varepsilon = 0.455$. Dividing by the time difference of $\Delta t = 4.66$ s between these two frames, a true strain rate of 0.09977 s^{-1} is obtained. For the particles 2 – 2 to 6 – 6, the determination of the true strain rates is listed in Table 2. It follows from the last column of this table that the true strain rate is in excellent agreement with the nominal strain rate, usually within 1%. Furthermore, this result shows that the reference length L_0 was determined correctly and that the sample was externally and internally quite homogeneous. Concerning the small difference between the true and the nominal strain rates, it should be noted that the uncertainty in the latter quantity is also about 1%.

[7]) These distances are not the true geometrical distances between the particles but are the distances measured on the print-outs obtained from the photoprinter. What matters here are the ratios between these distances such that the optical magnification has no influence.

Table 2. Determination of true strain rate from marks on sample. Test 93/7-19.2 (LDPE)

	Time [s]	Distance	L [mm]	Δt [s]	$\Delta\lambda$	$\Delta\varepsilon$	$\dot{\varepsilon} = \Delta\varepsilon/\Delta t$ [s^{-1}]
1	2.59	1–1	55.7				
2	7.25	1–1	87.8	4.66	1.576	0.455	0.0977
		2–2	48.6				
3	14.13	2–2	96.7	6.88	1.99	0.688	0.100
		3–3	27.1				
4	24.01	3–3	73.1	9.98	2.697	0.992	0.0994
		4–4	27.2				
5	34.81	4–4	77.8	10.80	2.868	1.053	0.0975
		5–5	41.3				
6	43.85	5–5	a)103.0	9.04	2.493	0.914	0.101
		5–5	b)101.6	9.04	2.460	0.900	0.0995
		6–6	58.0				
7	48.6	6–6	94.0	4.75	1.62	0.483	0.101_2

(d) Calculation of tensile stress

For tests at constant strain rate, the motors driving the clamps are switched-on at a pre-set, constant speed of rotation. The tensile force in the sample is then recorded as a function of time. Figure 14 shows the strip chart record of the force signal for a melt of a conventional polystyrene (Polystyrol 158 K of BASF Ludwigshafen, Germany) at a strain rate of $0.1\ s^{-1}$ and a temperature of 170 °C. The resulting strip has been cut into two pieces for preparing Fig. 14. On the lower piece there are two traces corresponding to two different sensitivities of the two channels used for recording. We notice that shortly

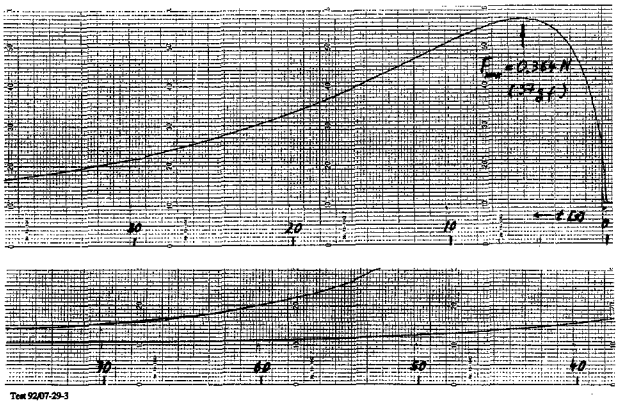

Fig. 14. Polystyrene melt extension: Record of tensile force. Polystyrol 158 K (pre-extruded); test temperature 170 °C, elongational strain rate $0.1\ s^{-1}$. The sample had been prepared from a sheet compression moulded from hot melt immediately after twin screw extrusion. At 170 °C the initial cross-sectional area of the sample is $A_0 = 15.9\ mm^2$

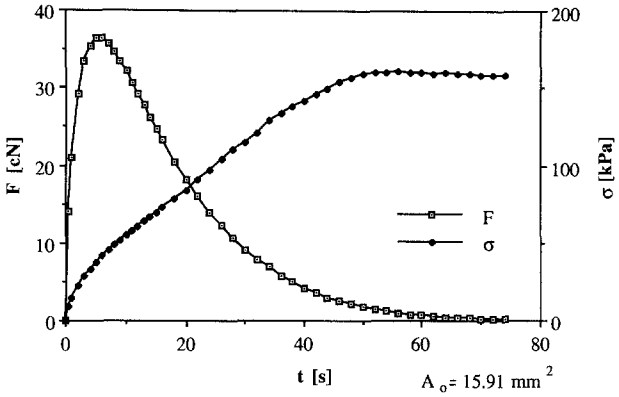

Fig. 15. Polystyrene melt extension: Record of tensile force and tensile stress for the same test as for Fig. 14

after the start of the force signal there is a maximum with $F_{max} = 0.364$ N (37 gf) followed by a gradual decrease of the force up to about 75 s when the maximum strain is reached.

In Fig. 15 the tensile force is re-plotted along with the tensile stress σ, both as functions of time. The tensile stress, $\sigma(t)$, is calculated from the measured force $F(t)$, the initial cross-sectional area A_0 at test temperature, and its variation during deformation, compare Fig. 2, such that

$$\sigma(t) = F(t)/A(t) = F(t)/A_0 \exp\{-\dot{\varepsilon}_0 t\} \ . \qquad (8)$$

(e) Influence of thermal expansion

The cross-sectional area A_0 at test temperature is determined from the sample height $H°$ and width $W°$, measured at room temperature (23 °C), and the thermal expansion of the specific volume v or the density ϱ. Specifically, we need $v(T)/v° = \varrho°/\varrho(T)$ where T is the test temperature and the superscript ° refers to room temperature. The following relation holds:

$$A_0 = H° W° [v(T)/v°]^{2/3} = H° W° [\varrho°/\varrho(T)]^{2/3}. \qquad (9)$$

At room temperature the dimensions of the sample used for Fig. 15 and 16 were $H° = 2.16$ mm and $W° = 7.05$ mm. For the specific volume of polystyrene[8]) we use $v(T = 170\,°C) = 1.017\ cm^3/g$ and

[8]) For polystyrene of high molecular weight above the glass transition temperature Ueberreiter and Kanig (1951) give the following relation for the temperature dependence of the specific volume: $v(T) = 0.7674 + 0.00055T\ cm^3/g$ (T in K), hence $v(170\,°C) = 1.011$. We measured the value 1.017 in our pvT apparatus (Gnomix Research, Boulder, Col., USA).

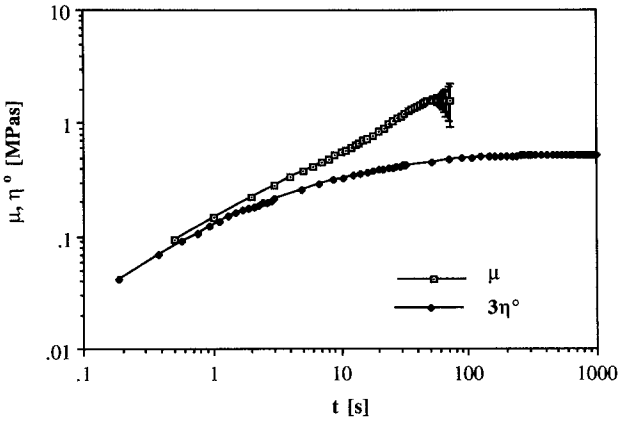

Fig. 16. Elongational viscosity for the same test and test conditions as for Fig. 14 and Fig. 15 and the three-fold of the linear viscoelastic shear viscosity. The latter has been measured in the RMS 800 at a shear rate of 0.001 s^{-1}

$v^\circ = 0.952\ cm^3/g$. From Eq. (9) it follows that $A_0 = 15.91\ mm^2$.

(f) Example of test result: Elongational viscosity of a polystyrene melt

We notice from Fig. 15 that after $t = 50$ s the stress becomes constant at a magnitude of approximately 0.15 MPa reflecting a constant value of the elongational viscosity after a total strain of $\varepsilon = \dot{\varepsilon}_0 t = 5$ Hencky units. We further notice that the total strain is more than $\varepsilon = 7$. This is a remarkably large total elongation that could be achieved only after the above described sample preparation technique had been developed (viz. shearing the melt followed by compression moulding).

Due to the exponentially decreasing cross-sectional area the force becomes very small at large strains so that the error of the stress record increases. Figure 16 shows the elongational viscosity $\mu(t)$ versus time in a double-logarithmic plot. Also shown in Fig. 16 is three times the linear viscoelastic transient (stressing) viscosity, $3\eta^\circ(t)$, which was measured in a Rheometrics Mechanical Spectrometer RMS 800 at a shear rate of 0.001 s^{-1}. We notice that at the onset of the stress growth, both material functions coincide, but that after a deformation time of 1 s, the elongational viscosity rises above the linear viscoelastic prediction, $3\eta^\circ(t)$.

6. Comparison of different polyethylene melts

For melts of lower viscosity, the tensile forces can be much lower than those shown in Fig. 15 and,

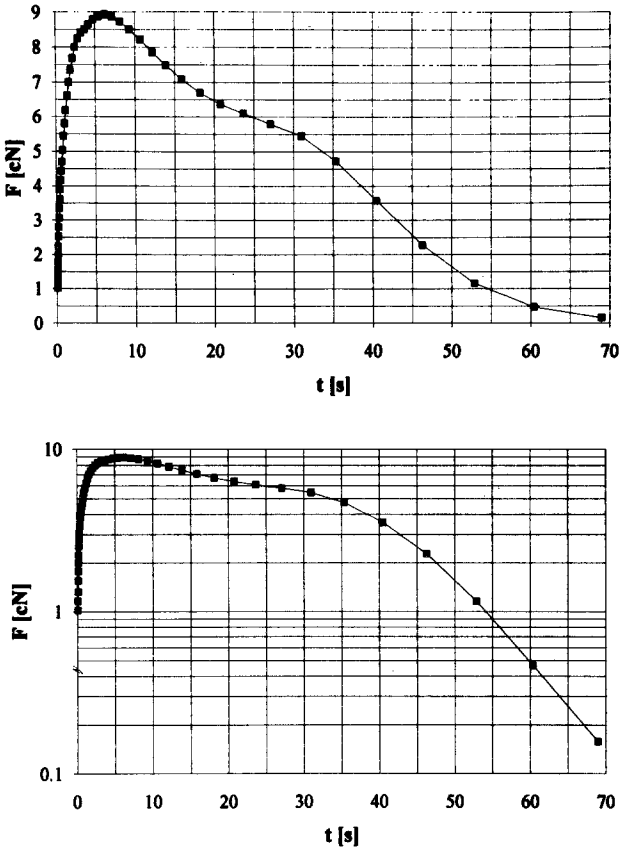

Fig. 17. LDPE melt elongation at a nominal strain rate of 0.1 s^{-1} and a temperature of 150 °C. Material: Lupolen 1810 H[9]. Above linear, below logarithmic plot of the measured force signal as a function of the deformation time t. Dimensions of the sample at room temperature: Width $W^\circ = 7.00$ mm, height $H^\circ = 2.09$ mm, ratio of the specific volumes at test and room temperature: $v(150\,^\circ C)/v(23\,^\circ C) = 1.2825/1.087 = 1.182$. The cross-sectional area at onset of test is $A_0 = 16.36\ mm^2$

therefore, the special belts with welded-on tongues (Fig. 7c) have to be used. This requires an adjustment of the driving speed control, because the basis length, L_0, increases during the first short period of elongation, during which the tongues are pulled into the gap between the metal belts. In this case the independent, visual verification of the test performance (elongation and strain rate) is vital.

Figure 17 shows the measured tensile force for a melt of a conventional low density polyethylene LDPE (LUPOLEN 1810 H[9]) of BASF, Germany) having a melt index (MFI 190/2.16) of 1.2 g/10 min (US standard ASTM D 1238-65T). The elongation

[9]) Charge 681 133 259.

was performed at a strain rate of $0.1\ s^{-1}$ and a temperature of 150 °C. It is the same test used in Fig. 13 to illustrate the determination of the true strain rate. The maximum force is only 8.9 cN (8.9 gf), and we notice a gradual decrease of the force signal after the maximum. This behaviour seems to be typical of LDPE, because for a sample of linear low density polyethylene (LLDPE) under the same conditions the force signal is remarkably different, as shown in Fig. 18 for the force in a melt of LLDPE (DOWLEX NG 5056 E[10]) of DOW-Europe, melt index 1.04 g/10 min). In fact, the maximum force is only slightly different, but afterwards the force decreases rather rapidly. This decrease is exponential, as can be seen from the lower, semi-logarithmic plot of Fig. 18. At 48 s, corresponding to a Hencky strain of 4.8, the force crosses the limit of 0.1 cN = 1 mN that is usually considered to be the lower limit of the force range of the rheometer. But we notice from the logarithmic force record that results down to 0.05 cN = 0.5 mN seem to be reasonable.

From the video record made during the LLDPE melt elongation of Fig. 18, the side views of the sample at different instants of time are shown in Fig. 19, together with the resulting true elongational strain rates. Again, as was the case for the LDPE results shown in Fig. 13, the agreement between the nominal and the true strain rate is excellent.

An impression of the reproducibility of the test results can be obtained by inspection of Fig. 20 which shows elongational viscosities $\mu(t)$ from three tests performed under the same test conditions for the LDPE melt, Fig. 21 shows data for the LLDPE melt from four tests.

From Figs. 20 and 21 follows that the reproducibility of the test results is very good. The elongational viscosities[11]) of the LDPE and the LLDPE samples together with that of a linear polyethylene HDPE (Lupolen 6011 L[12]) of BASF, melt index 4.9 g/10 min) are compared in Fig. 22. Also shown for each material is three times the linear viscoelastic shear viscosity $3\eta^\circ(t)$. $\eta^\circ(t)$ was determined by oscillatory shear using a Rheometrics Mechanical Spectrometer RMS 800. From the measured dynamic shear moduli, G' and G'', the transient viscosity $\eta^\circ(t)$ can be calculated by means of the following approximate relation derived by F. R. Schwarzl (1970) and published by Meissner (1972b):

$$\eta^\circ(t)/t = \{G'(\omega) + 0.27\,G''(2\omega) + 0.115\,G''(4\omega)\}_{\omega = 1/\tau} \,. \tag{10}$$

According to Schwarzl (1970), the maximum relative error of this relation is ±12%.

We see from Fig. 22 for all samples that at short times the elongational viscosity tends to follow the linear viscoelastic prediction, viz. $\mu(t) = \mu^\circ(t) = 3\eta^\circ(t)$, except for very short times, $t < 0.5$ s, where deviations are probably caused by start-up problems

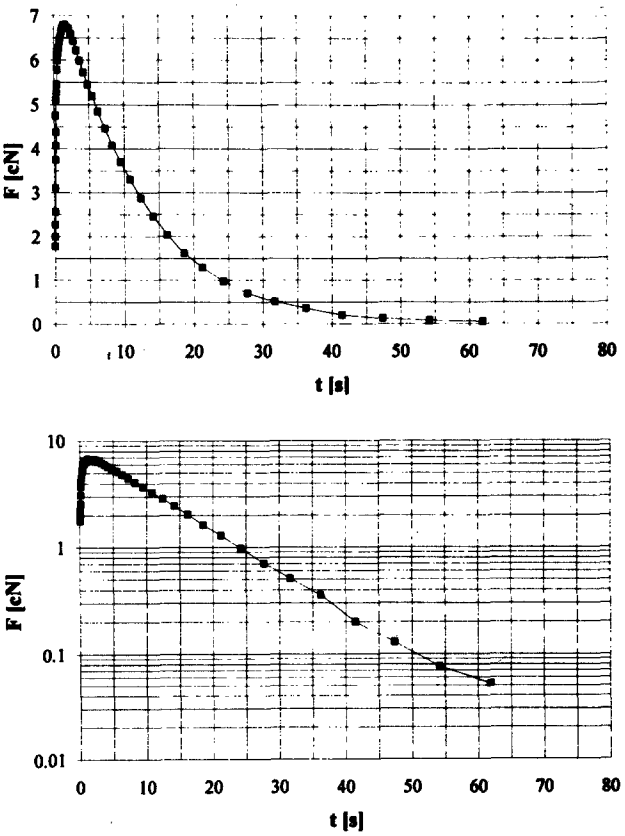

Fig. 18. Tensile force during LLDPE melt elongation, material: Dowlex NG 5056 E[10]. Test conditions as in Fig. 17. Sample dimensions at room temperature: Width $W^\circ = 7.02$ mm, height $H^\circ = 2.21$ mm. Ratio $v(150\,°C)/v(23\,°C) = 1.268/1.0875 = 1.1660$. Cross-sectional area at onset of test is $A_0 = 17.19\ mm^2$

[10]) Lot ET 93010222313 A.

[11]) For a quick consideration of the thermal expansion, we refer to Gubler and Kovacs (1959) who found that for polyethylene, independent of branching, the specific volume of the melt follows the relation $v(\theta) = 1.262 + 0.0009(\theta - 125)$ with θ in °C. From this relation we take $v(150\,°C) = 1.285\ cm^3/g$ for the LDPE. The LLDPE was measured in our pvT apparatus (Gnomix) and resulted in $v(150\,°C) = 1.268\ cm^3/g$. In the following we use this result for LLDPE.

[12]) Charge 657 303 216.

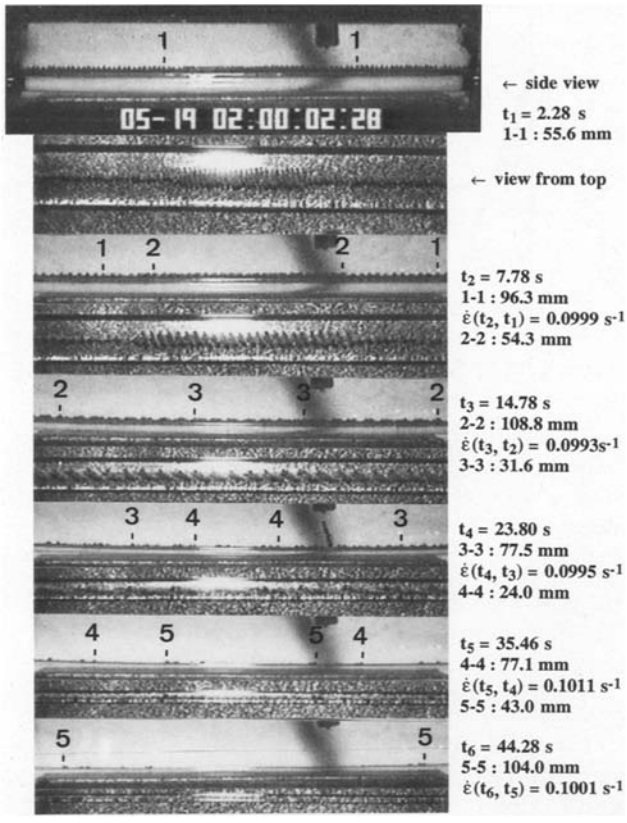

Fig. 19. Side views of the LLDPE sample during elongation in the same test used for Fig. 18. The indicated strain rates refer to the evaluation of the stretch between the same two markers of SiC powder during the indicated time difference, e.g. $\dot{\varepsilon}_3(t_3, t_2)$ refers to the stretch of particles 2 – 2 between t_3 and t_2: $\dot{\varepsilon}_3(t_3, t_2) = [\ln (108.8/54.3)]/(14.78\ \text{s} - 7.78\ \text{s}) = 0.0993\ \text{s}^{-1}$

of the rheometer that require more detailed investigation in the future[13]). However, the three samples show different degress of 'strain-hardening', i.e. an increase above $3\eta^+(t)$; these are different in magnitude and also different with respect to the time (or elongation) at which this hardening starts to occur. The remarkable early start of this hardening and the dramatic increase of $\mu(t)$ well above $3\eta^+(t)$ for the LDPE melt, including the existence of a well pronounced maximum, has been reported previously by Raible (1981) and Meissner et al. (1981). Raible used a different apparatus equipped with rotary clamps and a much different sample size. The material was the same, except that the lot (charge) number was different. It is noteworthy that Raible's result is in very good agreement with the curve measured 10 years later for the same LDPE and shown in Fig. 22.

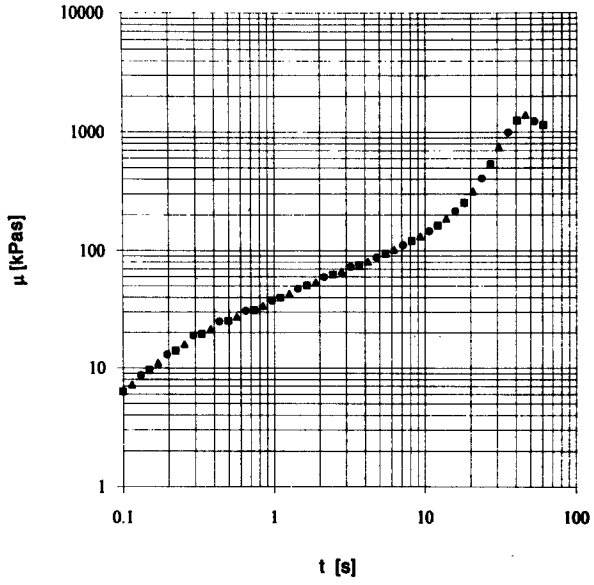

Fig. 20. Reproducibility of test results for the LDPE melt: Elongational viscosity $\mu(t)$ from three different tests. Same material and test conditions (nominal strain rate 0.1 s^{-1}) as for Fig. 13 and Fig. 17. The true strain rates are for the symbols ■: 0.0997 s^{-1}, ▲: 0.1008 s^{-1}, ●: 0.0998 s^{-1}

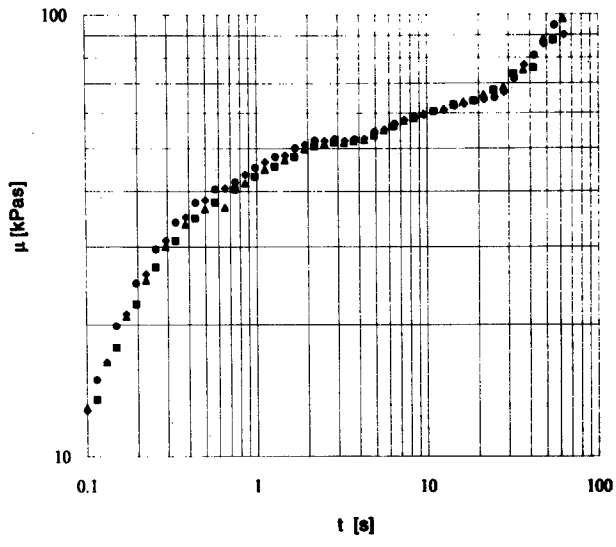

Fig. 21. Reproducibility of test results for the LLDPE melt. Elongational viscosity $\mu(t)$ from four different tests. Same material and test conditions (nominal strain rate) as for Fig. 18 and Fig. 19. The true strain rates are for the symbols: ■: 0.0952 s^{-1}, ●: 0.0962 s^{-1}, ▼: 0.0965 s^{-1}, ◆: 0.0945 s^{-1}

[13]) Similar start-up problems also occur in rotational rheometers, as has been discussed by Meissner (1972b).

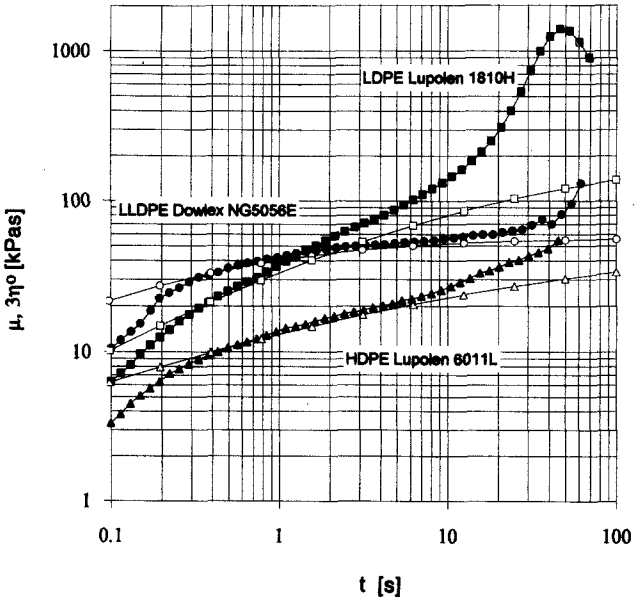

Fig. 22. Elongational viscosity of three melts of different polyethylenes measured at a nominal strain rate of 0.1 s^{-1} and a temperature of 150 °C. The open symbols refer to $3\eta°(t)$. $\mu(t)$ for the LDPE corresponds to the test used for the force curve of Fig. 17, the result for the LLDPE sample corresponds to the test for Fig. 18. For the HDPE sample the true strain rate is $\dot{\varepsilon} = 1.027\ s^{-1}$, the deviation from 0.100 s^{-1} had been caused by an incorrect fixing of the reference length L_0 at this test

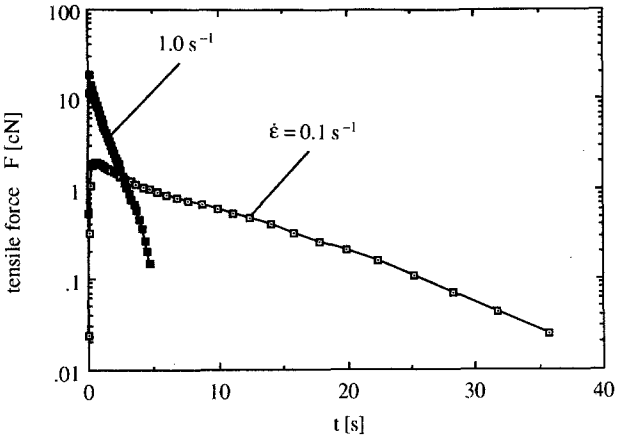

Fig. 23. Polyamide melt extension: Tensile force as a function of time at strain rates of 0.1 and 1 s^{-1} and a temperature of 250 °C; polyamide-6 (Ultramid B4 of BASF). Initial dimensions of the samples at room temperature are for $\dot{\varepsilon}_0 = 0.1\ s^{-1}$: Width $W° = 6.98$ mm, height $H° = 2.3$ mm, and for $\dot{\varepsilon}_0 = 1\ s^{-1}$: $W° = 6.93$ mm, $H° = 2.8$ mm. The initial cross-sectional areas are $A_0 = 17.70\ mm^2$ (for 0.1 s^{-1}) and $A_0 = 21.40\ mm^2$ (for 1 s^{-1})

In contrast to the LDPE, the curve of the LLDPE follows the linear viscoelastic $3\eta°(t)$ for a much longer period. It takes approximately 30 s (or 3 Hencky strain units) for a remarkable increase to start. Surprisingly, the HDPE melt also deviates from $3\eta°(t)$, but starts to do so at a shorter time and more smoothly. It should be added that using the sample preparation method described, the HDPE sample could be elongated without any difficulty up to large elongations. The viscosity representation of Fig. 22 for the HDPE selected was terminated at $t = 46$ s, because the measured force decreased below the lower limit of the force range of the rheometer.

7. High temperature results

In this section, results are reported that were obtained above 200 °C which had previously been considered to be the upper temperature limit for polymer melt elongational rheometry. With the new instrument, measurements have been performed without problem up to 350 °C.

Figure 23 shows the forces resulting from elongating a polyamide 6 melt at a temperature of 250 °C at two strain rates. The material is a commercial product (Ultramid B4 of BASF, Germany). For the calculation of the initial cross-sectional area, we used the following ratio of the densities[14]) at room temperature and at the test temperature: $\varrho(20\,°C)/\varrho(250\,°C) = 1.135/0.98 = 1.158$.

We notice that at the same strain rate of $\dot{\varepsilon}_0 = 0.1\ s^{-1}$ the tensile force is less than half of those shown in Fig. 17 or Fig. 18. In spite of the high temperature, the forces can be reliably measured and the viscosity determined; the latter is plotted in Fig. 24. We notice that the elongational viscosity becomes approximately constant at 0.1 s^{-1} but shows a definite increase ("strain hardening") at 1 s^{-1}.

The next two figures show test results obtained for a poly(ethersulfone) sample. The ratio of the densities at room temperature and at the test temperature of 350 °C is $\varrho(20\,°C)/\varrho(350\,°C) = 1.37/1.31 = 1.046$[15]). Because of the low viscosity, it was sufficient to use only the lower belts, in other words the test was per-

[14]) The density as a function of temperature for polyamide 6 has been published in Technisches Merkblatt Ultramid B-Marken of BASF (May 1978). From this we take $v(250\,°C)/v(23\,°C) = \varrho(23\,°C)/\varrho(250\,°C) = 1.135/0.98 = 1.158$.

[15]) Information from Dr. H. M. Laun of BASF Aktiengesellschaft, Ludwigshafen am Rhein, Germany

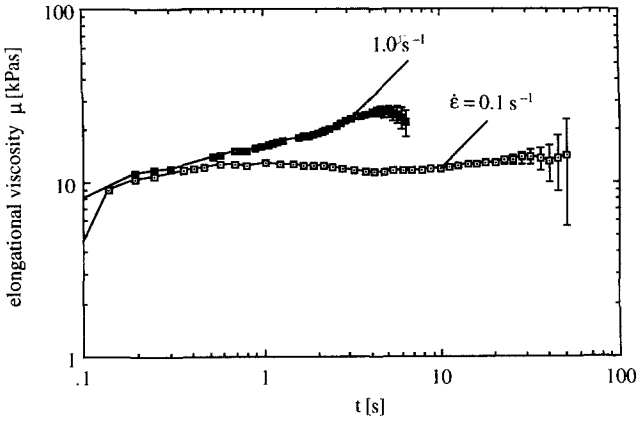

Fig. 24. Polyamide melt extension: Elongational viscosity at 250 °C. Same test conditions and material as in Fig. 23

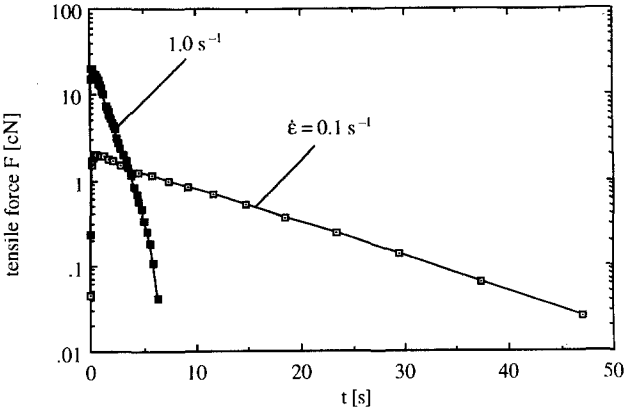

Fig. 25. Melt extension of poly(ethersulfone) (Ultrason E 6010 of BASF) at 350 °C, strain rates $\dot{\varepsilon}_0 = 0.1$ and $1\ s^{-1}$. Sample dimensions at $0.1\ s^{-1}$: $W° = 7.02$ mm, $H° = 1.81$ mm, $A_0 = 13.43\ mm^2$; at $1\ s^{-1}$: $W° = 7.01$ mm, $H° = 1.84$ mm, $A_0 = 13.64\ mm^2$. At $\dot{\varepsilon}_0 = 1\ s^{-1}$ the clamping was performed by the lower belts only as shown in Fig. 8c

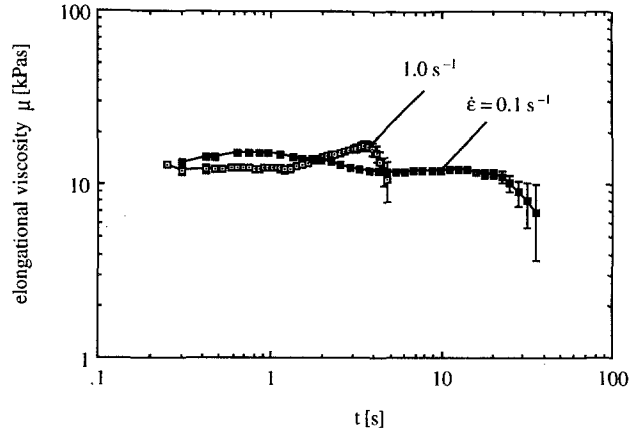

Fig. 26. Elongational viscosity of poly(ethersulfone). Test conditions and material as for Fig. 25

formed by using the configuration (c) of Fig. 8. Figure 25 shows the forces measured and Fig. 26 the elongational viscosity. We notice that the viscosity is practically constant and independent of strain rate. The error bars in Fig. 26 reflect the noise in the force record. This noise becomes large when the force is below the limit of 1 mN. Sample preparation is difficult, and we are grateful to Dr. H.M. Laun of BASF who sent us well-prepared samples.

8. First tests with bread dough

The new rheometer can be used for elongational measurements not only with polymer melts but also with other materials of similar viscoelastic properties. As an example of a very different class of materials, we collaborated with Professor F. Escher[16]) and his co-workers to perform elongational measurements on samples of bread dough. As in the case of polymer melts, with bread dough the careful preparation of the samples is extremely important. The standard dough is prepared by kneading; then sheets are rolled out, and, after a period of 90 min, samples are cut from the sheets. Before introducing a sample into the instrument, it was covered by a wax (food grade coating) in order to avoid drying and adhesion during manipulation to fix the sample into the clamps.

Figure 27 shows the force measured during the elongation of two samples with and two samples without ascorbic acid, at a strain rate of $0.06\ s^{-1}$ and a temperature of 25 °C. The force signals for the two

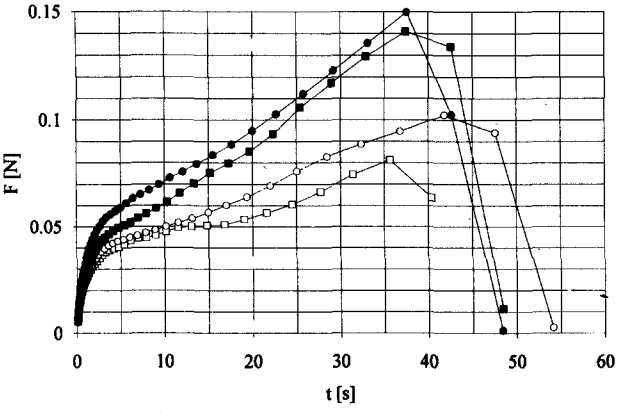

Fig. 27. Extension of bread dough with (■, •) and without (□, ○) ascorbic acid. Sample dimensions $H° = 2$ mm, $W° = 7$ mm; elongational strain rate $0.06\ s^{-1}$, temperature 25 °C

[16]) Professor Dr. F. Escher, Institut für Lebensmittelwissenschaft of ETH Zürich.

samples of each kind do not completely coincide, but this cannot be expected because with bread dough as a 'living system' the mechanical and thermal (including environmental) pre-history of each individual sample is extremely important and might be slightly different. More details on the dough and the sample preparation technique and more results (obtained also at other strain rates) will be published in a forthcoming paper by Prof. Escher.

From Fig. 27 we notice that there is a steady increase of the force F up to a sudden decrease at approximately $t = 40$ s, corresponding to 2.4 Hencky strain units ($\lambda \approx 11$). At this elongation, the sample starts to neck or even shows fracture. Consequently, the evaluation of the elongational viscosity has been performed only up to this force maximum. Noteworthy is the influence of the ascorbic acid, viz. an increase of the tensile force of a little more than 50% relative to the standard dough without ascorbic acid. The elongational viscosities obtained from the four samples are shown in Fig. 28. From this result it follows that bread dough also shows a well-developed strain hardening behaviour and that the viscosity falls well within the range that can be measured in the new rheometer.

9. Appendix: Influence of surface tension

For an elongational rheometer in which the polymer melt floats on a supporting liquid, e.g. polyethylene on silicone oil, the error in the measured force caused by the interfacial tension between the melt and the liquid was shown by Meissner (1971) and Laun and Münstedt (1978) to be negligible. However,

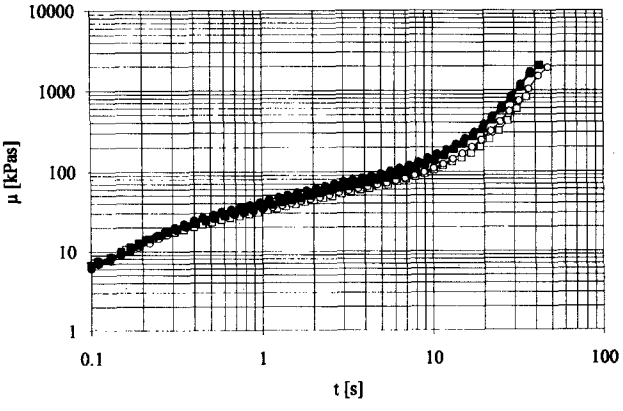

Fig. 28. Elongational viscosity of bread dough with and without ascorbic acid. Test conditions and sample identification are the same as in Fig. 27

in the new rheometer the 'supporting liquid' is nitrogen or argon and the surface tension is much larger. Furthermore, due to the rectangular shape of the cross-section, the surface/volume ratio is greater, and the force resolution allows us to measure lower forces than previously. For these reasons, the question of a correction of the measured tensile stress for the surface tension has to be re-considered. We start the discussion with a short repetition of the previous results:

For a sample of circular cross-section of current radius, a, and interfacial tension, α (between silicone oil as supporting liquid and the polymer melt), the total work per unit time dW/dt consists of two parts. For the viscoelastic deformation the work is $\sigma_{\text{def}} \dot{\varepsilon}_0 \pi a^2 L_0$, and for the increase in interfacial area the work is $\alpha \dot{\varepsilon}_0 \pi a L_0$. If σ is the measured tensile stress, one obtains Eq. [15] of Meissner (1971):

$$dW/dt = \sigma \dot{\varepsilon}_0 \pi a^2 L_0 = \sigma_{\text{def}} \dot{\varepsilon}_0 \pi a^2 L_0 + \alpha \dot{\varepsilon}_0 \pi a L_0 \ . \tag{11}$$

From the measured stress σ, only the portion σ_{def} should be used for the calculation of the elongational viscosity μ. Hence, the following correction for the stress must be made:

$$\sigma_{\text{def}} = (1 - \alpha/a\sigma)\sigma \ . \tag{12a}$$

Since $\pi a^2 \sigma$ represents the tensile force, F, directly measured, we can also write

$$\sigma_{\text{def}} = (1 - \pi a \alpha / F)\sigma \ . \tag{12b}$$

Hence, if the surface tension is neglected, the systematic relative error is

$$\Delta\sigma/\sigma = (\sigma - \sigma_{\text{def}})/\sigma = \pi a \alpha / F \ . \tag{12c}$$

For the elongation of a polymer melt in silicone oil, Meissner (1971) calculated the maximum error to be 5% for the smallest strain rate he used (0.001 s^{-1}), a radius of 1 mm, and a tensile viscosity of 0.1 MPas (reflecting a tensile stress of 100 = Pa 1000 dynes/cm^2).

In the new rheometer the polymer melt is supported by gas such that α is now the surface tension (of the order of 30 dynes/cm^2). Furthermore, the surface area is larger because of the rectangular cross-section. Therefore, under certain conditions, a correction may be required when the total stress, σ, is set equal to σ_{def}. The height H and width W of the sample change dur-

ing deformation according to $H = H_0 \exp(-\dot{\varepsilon}_0 t/2)$ and $W = W_0 \exp(-\dot{\varepsilon}_0 t/2)$, respectively. Hence, the rate of change of the surface area $S(t) = 2[H(t) + W(t)]L_0(t)$ between the clamps is

$$dS/dt = 2(H_0 + W_0)(\exp(-\dot{\varepsilon}_0 t/2)\, dL_0/dt + 2(H_0 + W_0)L_0(-\dot{\varepsilon}_0/2)\exp(-\dot{\varepsilon}_0 t/2). \quad (13)$$

With $dL_0/dt = L_0(dL_0/L_0)/dt = L_0\dot{\varepsilon}_0$, we finally obtain

$$dS/dt = (H_0 + W_0)L_0\dot{\varepsilon}_0 \exp(-\dot{\varepsilon}_0 t/2)\ . \quad (14)$$

Hence, for the total force measured, Eq. (9) has to be re-written for the rectangular cross-section as follows:

$$dW/\mathrm{dt} = \sigma\dot{\varepsilon}_0 HWL_0 = \sigma_{\mathrm{def}}\dot{\varepsilon}_0 HWL_0 + \alpha\dot{\varepsilon}_0(H + W)L_0\ . \quad (15)$$

From the right-hand equation of (15) it follows with the tensile force $F = \sigma HW$ that

$$\sigma_{\mathrm{def}} = [1 - \alpha(H + W)/\sigma HW]\sigma = [1 - \alpha(H + W)/F]\sigma\ . \quad (16a)$$

The systematic relative error is

$$\Delta\sigma/\sigma = (\sigma - \sigma_{\mathrm{def}})/\sigma = \alpha(H + W)/F\ . \quad (16b)$$

From Eq. (16b) it follows that the error is large at large values of H and W and at small values of the tensile force F. For a quick estimate of the error, we use as the small tensile force the minimum of the force range of the present spring system in the rheometer, viz. $F = 0.1$ cN $= 100$ dynes and make the estimate for two examples, viz. the results of Fig. 18 (for the LLDPE) and Fig. 23 (for the polyamide). In both cases we assume for the surface tension the value $\alpha = 30$ dynes/cm.

Example 1: In Fig. 18, the tensile force of 0.1 cN occurs at a deformation time of about $t = 50$ s. The initial dimensions of the sample at room temperature are $H° = 2.21$ mm and $W° = 7.02$ mm. Due to thermal expansion these dimensions have to be multiplied by the factor $v[(150\,°\mathrm{C})/v(23\,°\mathrm{C})]^{1/3} = [\varrho(23\,°\mathrm{C})/\varrho(150\,°\mathrm{C})]^{1/3} = [0.92/0.779]^{1/3} = 1.057$. Therefore, at the start of the elongation the initial dimensions are $H_0 = 2.34$ mm and $W_0 = 7.42$ mm, and at $t = 50$ s, the required sum $H + W = (H_0 + W_0)\exp\{-\dot{\varepsilon}_0 t/2\} = 9.76 \exp(-2.5)$ mm $= 9.76 \times 0.082 = 0.80$ mm $=$ 0.08 cm. Inserting this information into Eq. (16b), the resulting error is $\Delta\sigma/\sigma = \alpha(H+W)/F = 30 \times 0.08/100 = 0.024 = 2.4\%$.

Example 2: From Fig. 23 the polyamide melt at 250 °C and $\dot{\varepsilon}_0 = 1\ \mathrm{s}^{-1}$ has a tensile force of 0.1 cN = 100 dynes at $t = 6$ s. The sample dimensions at room temperature are $H° = 2.8$ mm and $W° = 6.93$ mm. The multiplication factor due to thermal expansion is $[\varrho(23\,°\mathrm{C})/\varrho(250\,°\mathrm{C})]^{1/3} = [1.135/0.98]^{1/3} = 1.050$. Therefore, at the start of the elongational test, we have $(H_0 + W_0) = 1.02$ cm. At $t = 6$ s, $\exp\{-\dot{\varepsilon}_0 t/2\} = 0.05$. Hence the error $\Delta\sigma/\sigma = 30 \times 1.02 \times 0.05/100 = 1.5\%$.

From these examples it follows that the surface tension can be neglected if the elongational viscosities and the initial dimensions are similar to the dimensions used in these examples and an error of 3% can be tolerated.

10. Conclusions and Outlook

The main conclusion of this paper is that with the new elongational rheometer most of the remaining problems in polymer melt elongational rheometry and also in elongating other viscoelastic materials (example: bread dough) have been solved. The important features of the new instrument are as follows:

a) Only a small amount of materials is required for one sample. (This opens the way for an efficient investigation of structure-melt properties relationships.)
b) The operation of the instrument is easy.
c) The test performance can be verified and documented (recorded on video).
d) There is a broad range of strain rates and a high resolution of the force measured.
e) The maximum temperature of 350 °C used so far is outstanding, the problem of the environment is solved by supporting the sample on an inert gas.
f) The results obtained for various polymers and different conditions prove that the test conditions (especially the test temperature) can be changed without difficulty.

When new materials are to be tested, there is often much more time required for learning how to prepare good samples than for performing the elongational measurements, because, and this cannot be emphasized often enough, the quality of the test results depends not only on the performance of the instrument but also on the quality of the sample. The ideal

sample should be isotropic and externally (geometrically) and internally (molecular connectivity) homogeneous. It goes without saying that there should be no bubbles included nor gas dissolved in the sample.

For heterogeneous materials, e.g. glass-filled polymers or polymer blends, the deformation is often inhomogeneous. This is not always the fault of the rheometer or the operator but can be caused by the distribution of the different phases and the mixing procedure[17]. When the elongation becomes inhomogeneous (for homogeneous samples the reason often is an inhomogeneous temperature field), any data processing becomes questionable.

The determination of the true strain rate from the video record by using marks on the sample is especially important. We repeat that an error in the strain rate of 1% produces an error in the calculated stress of at least 7% at an elongation of 7 Hencky strain units. The same error follows for the elongational viscosity.

Finally we point out that in connection with the new rheometer problems still exist that have to be worked out in the future. We name the following:

(1) Analysis and improvement of the start-up behaviour.
(2) Change of strain rate during a test to permit, for example, stress relaxation after cessation of constant strain rate flow.
(3) Modification of the drive software such that creep measurements (flow with constant stress) can be performed.
(4) Design of device for performing recovery after melt extension.
(5) Application of the experience described here for simple elongation to the design and construction of an apparatus capable of performing other modes of elongation, e.g. equibiaxial, planar, etc.

In spite of these remaining problems, we believe that the present version of the new instrument is an important step forward in elongational rheometry.

Acknowledgement

Many co-workers have helped us in the development of the new elongational rheometer and the performance of measurements. We express our thanks to the following individuals: Peter Hachmann, Dr. Josif Leikin, Fredy Mettler, Heinz Oesch, Werner Schmidheiny, Dr. Thomas Schweizer, and Dr. Breda Zerjal. For the donation of the test material we are thankful to BASF Aktiengesellschaft, Ludwigshafen am Rhein, Germany, and to DOW Chemical Europe S.A., Horgen, Switzerland and Terneuzen, Holland. Finally, we thank Professor J. Dealy for transforming our manuscript into a much better readable English.

[17]) One method for characterizing the morphology of the melt of a blend is to rapidly quench the sample and make micrographs, as has been performed after elongating melts of polystyrene/poly(methylmethacrylate) blends by Gramespacher (1993) and reported by Meissner (1992b).

References

Ballman RL (1965) Extensional flow of polystyrene melt. Rheol Acta 4:137 – 140

Cogswell FN (1968) The rheology of polymer melts under tension. Plastics & Polymers 36(4):109 – 111

Dealy JM (1990) Do polymeric liquids exhibit strain hardening? J Rheol 34:1133 – 1147

Jenckel E, Ueberreiter K (1938) Ueber Polystyrolgläser verschiedener Kettenlänge. Z physikal Chem A 182:361 – 383

Gramespacher HF (1993) Einfluß der Grenzflächenspannung auf das rheologische Verhalten von Schmelzen aus Polystyrol/Polymethylmethacrylat-Mischungen in Dehn- und Scherströmung. PhD thesis Nr. 10179 ETH Zürich

Gubler MG, Kovacs AJ (1959) La structure du polyéthylène considére comme un mélange de n-paraffines. J Polymer Sci 34:551 – 568

Karam HJ, Bellinger JC (1964) Tensile creep of polystyrene at elevated temperatures. Part I. Trans Soc Rheol 8:61 – 72

Laun HM, Münstedt H (1978) Elongational behaviour of a low density polyethylene melt. I. Strain rate and stress dependence of viscosity and recoverable strain in the steady state. Comparison with shear data. Influence of interfacial tension. Rheol Acta 17:415 – 425

Meissner J (1969) Rheometer zur Untersuchung der deformations-mechanischen Eigenschaften von Kunststoff-Schmelzen unter definierter Zugbeanspruchung. Rheol Acta 8:78 – 88

Meissner J (1971) Dehnungsverhalten von Polyäthylen-Schmelzen. Rheol Acta 10:230 – 242

Meissner J (1972a) Development of a universal extensional rheometer for the uniaxial extension of polymer melts. Trans Soc Rheol 16:405 – 420

Meissner J (1972b) Modifications of the Weissenberg rheogoniometer for measurement of transient rheological properties of molten polyethylene under shear. Comparison with tensile data. J Appl Polym Sci 16:2877 – 2899

Meissner J (1985) Experimental aspects in polymer melt elongational rheometry. Chem Eng Comm 33:159 – 180

Meissner J (1987) Polymer melt elongation – methods, results, and recent developments. Polymer Eng & Sci 27:537 – 546

Meissner J (1992a) Conventional and new test modes in polymer melt rheometry, Chap 6 (p. 201 – 230) in: Mitchell J (ed) Applied Polymer Analysis and Characterization. Hanser Publishers Munich

Meissner J (1992b) Experimental problems and recent results in polymer melt rheometry. Makromol Chem, Macromol Symp 56:25 – 42

Meissner J, Raible T, Stephenson SE (1981) Rotary clamp in uniaxial and biaxial extensional rheometry of polymer melts. J Rheol 25:1 – 28, 673 – 674

Meissner J, Stephenson SE, Demarmels A, Portmann P (1982) Multiaxial elongational flows of polymer melts – classification and experimental realization. J Non-Newtonian Fluid Mechanics 11:221 – 237

Münstedt H, Laun HM (1979) Elongational behaviour of a low density polyethylene melt. II. Transient behaviour in constant stretching rate and tensile creep experiments. Comparison with shear data. Temperature dependence of the elongational properties. Rheol Acta 18:492 – 504

Petrie CJS (1979) Elongational Flows. London, Pitman, 254 pp

Raible T (1981) Deformationsverhalten von geschmolzenem Polyäthylen im Zugversuch bei großen Gesamtdehnungen. PhD dissertation Nr. 6751, ETH Zürich

Schwarzl FR (1970) Private communication

Ueberreiter K, Kanig G (1951) Die Kettenlängenabhängigkeit des Volumens, des Ausdehnungskoeffizienten und der Einfriertemperatur von fraktionierten Polystyrolen. Z Naturforsch 6a:551 – 559

Vinogradov GV, Leonov AI, Prokunin AN (1969) On uniaxial extension of an elasto-viscous cylinder. Rheol Acta 8(4):482 – 490

Zülle B, Linster JJ, Meissner J, Hürlimann HP (1987) Deformation hardening and thinning in both elongation and shear of a low density polyethylene melt. J Rheol 31:583 – 598

(Received October 22, 1993;
in revised form December 13, 1993)

Correspondence to:

Prof. Dr. J. Meissner
Institut für Polymere der ETH Zürich
ETH-Zentrum, ML J 21
8092 Zürich
Switzerland